Title

Additive Manufacturing Structural Redesign of Hip Prostheses for Stress-shielding reduction and improved Functionality and Safety

Authors

Gabriele Cortis[1], Ilaria Mileti[2], Filippo Nalli[1], Eduardo Palermo[1] and Luca Cortese[1]

Affiliations

[1]Department of Mechanical and Aerospace Engineering, Sapienza University of Rome, 00185 Rome, Italy.

[2]Department of Engineering, Mechanical Measurements and Microelectronics Laboratory (M3-Lab), University Niccolò Cusano, Rome, 00166, Italy

Contact Info

gabriele.cortis@uniroma1.it

Abstract

Nowadays, the total hip arthroplasty (THA) is a widespread surgical procedure, as the best option to restore hip joint mobility in patients suffering from trauma or joint diseases. One of the well-known possible drawbacks of THA is the stress-shielding phenomenon. Some years after the surgery, the femur starts to degrade because of its persistent unloaded condition induced by the high prosthesis stiffness, which carries the great part of the load normally taken by the bone. This condition is particularly invalidating in younger patients, with longer life expectation after the operation, requiring one or multiple additional operations to restore the proper prosthesis-bone firm connection.

The present study tries to address this issue proposing an innovative prosthesis design, taking advantage of the shape freedom ensured by Additive Manufacturing techniques. Additionally, the structural integrity of the novel prosthesis is assessed using a ductile damage numerical approach.

Different prosthesis geometries were investigated: one conventional and commercially available already, and two more innovative geometries. For each one, a bulk solution was compared to a lighter version characterized by an inner reticular structure with a body-centred cubic unit cell and by an equivalent density of about 5%, only feasible through the additive manufacturing fabrication.

Extensive Finite Element numerical simulations were carried out to compare the percentage of the induced stress shielding for the different prosthesis geometries. Pros and cons of each geometry were pointed out and eventually the most promising solution in limiting the stress shielding phenomenon was chosen. At the same time, the structural integrity of the selected design was ensured, embedding a ductile damage model in the Finite Element analysis, calibrated on a SLM Ti6Al4V, the biocompatible alloy for the prosthesis fabrication. Structural safety was evaluated under four different loading conditions: walking, stumbling, the exceptional overload due to hammering insertion during surgery and the force which induced the collapse of the implant. Additionally, the safety margin was quantified through the definition of an overall safety factor under the maximum expected load.

Keywords

Additive Manufacturing, Hip Prosthesis, Finite Element Analysis, Lattice Structure, Stress Shielding

Introduction

About one million worldwide sufferings of osteoarthritis experienced total hip arthroplasty (THA) during life. Defined as "the operation of the century", the THA represents the main surgical intervention used to restore motor functionality of patients suffering from trauma or severe joint diseases when conservative treatments have failed [1]. By 2030 the number of THA interventions is expected to significantly grow since the age at the primary intervention is trendy decreasing and the global population in older aged is projected to triple [2].

As of today, stress shielding and bone resorption are the main drawbacks of cementless THA, hampering the long-term survivorship of prostheses and increasing the risk of revision interventions [3]. The mismatch of mechanical properties between the surrounding living bones and the implant leads to an incorrect load distribution across the human kinematics, favouring bone resorption. Due to the stiffer nature of metal materials used, such as the titanium-based alloys, cobalt-chromium molybdenum alloys (CoCrMo), and 316L stainless steel, the physiological load primarily acts on the implanted stem, leaving the more compliant bone tissue unstressed. According to Wolff's law, a long-term adaptation response of the bone structure and density occurs to match the novel mechanical needs, due to alternation in mechanical stimuli of the overall system [3]. Various complications can occur when bone loss secondary to the stress shielding phenomenon starts damaging living bone tissues, including thigh pain, peri-prosthetic fracture as well as a reduction in the remaining bone quality. In this scenario, several designs have been studied to reduce the stress shielding phenomenon in the last decades [4].

In the majority of cases, research studies are mainly focused on the reduction of femoral stem stiffness through the optimization of implant structure and surface geometry. Different stem lengths and stem cross-sections, various shapes of the proximal attachment of collar or anchor, superficial grooves and curves, are some of those structural modifications that were considered in the stem design. In 2011, Khanuja et al. proposed a classification of traditional femoral stems by identifying an overall of six types according to implant geometry and fixation zones [5]. All stems were full components with a tapered, cylindrical or rectangular cross-section profile and with a partially or fully Hydroxyapatite-coated superficial layer. To reduce implant stiffness, multiple splines and/or grits were often raised through the implant longitudinal axis. From other literature studies, a shortened stem design was proposed, since implants with metaphyseal fixation performed better compared to those with surface-treated throughout the whole implant [6]. Despite the so-called metaphyseal stems report mini-invasive implantation with a higher long term osteointegration rate, its applicability is reduced. In fact, in the case of hip dysplasia, the anteverted fixation of the implant in the femoral neck could cause an adverse prosthesis displacement [7]. From literature findings, the most used traditional stem geometry consists of a full component with a single wedge coated in the wide proximal part along with an inclined slope of the proximal part and anterior/posterior sides on the distal portion [8]. Despite the external structural modification, Young's modulus of the traditional hip implants is still higher compared to one of the cortical and trabecular tissue bones, resulting in stress shielding effects.

With the advantages of Additive Manufacturing (AM) and the metal 3-D printing technologies, research efforts are focused on further lightening the femoral stem, by internally design its geometry. Modelling femoral components using AM techniques, not only raise the opportunity to lighten external and internal structures to satisfy physical and mechanical requirements, but also provides the means to leverage the implant space towards more functional outcomes. In this context, the mechanical properties of the femoral stem can be modified by internally varying structural spaces through a more bio-fidelity design involving pores [9], [10], lattices [11], [12], or trabeculae [13]. A lightweight CoCrMo monoblock with a porous topography of outer skin and an inner graded orthotropic porous structure was proposed by Hazlehurst et al, to match the mechanical properties of living femoral bone [9]. Results reported that functionally graded design can significantly improve stress distribution, especially in the medial and lateral perioprosthetic Gruen zones when compared to the traditional fully dense stem. A fully porous with inner thetraedus topology were introduce by Arabnejad et al. in 2017, to obtain an optimum density distribution among the entire implant [10]. The amount of bone loss secondary to stress shielding was estimated to be 75% less with respect to the bulky counterpart. In addition, computed tomography analysis has reported the mechanical integrity of inner cells and the absence of entrapped unmelted powder. Another AM design was proposed by Delikanli et al. in 2019. A solid lattice structure with variable sizing in the inner part and semi-spherical pores in the outer region was modelled and manufactured [14]. A reduction of 15-17% of the implant mass was obtained and the proposed manufacture reports enough fatigue performance according to the requirements of the ISO 7206 standard. In the study of Aversa et al., a biomimetic model of trabeculae implant is proposed, since the femoral calcaneus bones are mainly composed of isotropic and orthotropic shapes [13]. Five iso-rigidity regions combined with iso-tension lines were adopted in the design

to vary the elastic modulus across the stem. To redefine stress and strain distribution, iso- and ortho- structures were also adopted in the stem and femoral regions, respectively.

Though present studies report high-quality solutions, some issues have not yet been addressed satisfactorily. Current studies are mainly based on the numerical investigation of different femoral topography using mechanical characteristics of commercial Ti6Al4V and considering conventional loading tests. The recent introduction of Selective Laser Melting (SLM) for the rapid manufacture of Ti6Al4V through additive manufacturing technologies has led to different mechanical performances of AM titanium alloy compared to conventional counterparts. Modelling the inner trabecular stems without taking into account the mechanical properties of AM Ti6Al4V could lead to unsafe or at least non-optimized outcomes. In addition, for the analysis of the structural integrity of the implant, a damage model for ductile materials properly calibrate to Ti6Al4V SLM is also required for the prediction of material fracture onset and ultimate strength [15].

In the present study, an accurate parametric Finite Element (FE) model of a Ti6Al4V THA implant is setup to redesign a conventional hip prosthesis taking advantage of AM technology, to address bone resorption consequent to the stress shielding phenomenon while granting, at the same time, the proper structural integrity of the implant itself.

The prosthesis components will be designed with inner lattice structures, and an optimization of geometrical parameters will be issued to find the most effective solution. For the structural assessment of the Ti6Al4V SLM, the experimental results of a mechanical characterization of the Ti6Al4V SLM already published in a previous study by Nalli et al. [16] will be used in the Finite Element Analysis (FEA). In the latter, based on experimental data and inverse methods, the material stress-strain curve up to large strain was identified, and a damage model for the Ti6Al4V SLM was calibrated and validated. The stress-strain curve will be used here to tune the isotropic hardening model of the FE code, while the damage model will be implemented in the FE code by means of a custom subroutine to simulate the elastic-plastic collapse of the prosthesis under critical loads. Another crucial aspect that will be taken into account, which is not exhaustively examined by previous literature studies, is the analysis of actual loads acting on the prosthesis-bone system in every day and accidental scenarios, such as during the surgical insertion of the femoral stem or accidental falls.

Material and Methods

Materials and numerical model

Among the available additive metal alloys the titanium alloy Ti6Al4V manufactured via Selective Laser Melting (SLM) was chosen for its high strength and bio-compatibility as the best option to realize the prosthesis. It is worth noting how the same titanium alloy produced with standard technologies (i.e. not additive) is already wide-spreading in biomedical applications, while only in recent years the additive manufacturing techniques were employed for prostheses fabrication [17], [18]. As already stated, the authors' know-how was here exploited, using data coming from a previous characterization campaign on SLM Ti6Al4V [16]. In the authors' previous study, an EOS M290 SLM machine [19] was adopted to build the specimens used for the material characterization. The metal powder was provided by EOS itself; in the following Table 1 the chemical composition of the alloy is reported, while in Table 2 the mechanical properties as declared by the supplier are summarized.

Table. 1 Chemical composition of metal powders employed for AM specimens production.

Material	Al	V	O	C	N	H	Fe	Ti
Ti6Al4V	6	4	<0.15	<0.08	<0.04	<0.012	<0.250	Bal

Table. 2 Mechanical properties of SLM Ti6Al4V as declared by EOS GmbH. All the values refer to not heat-treated conditions. Vertical direction is perpendicular to the machine plate.

Material	Yield strength [MPa]	UTS [MPa]	Elongation at fracture [%]
Ti6Al4V(vertical)	1120±80	1240±50	10±3
Ti6Al4V (horizontal)	1140±50	1290±50	7±3

In order to assess the structural behavior of the redesigned prosthesis through FEA investigation, data coming from a previous experimental campaign [16] were used, as further detailed in the following. The accurate identification of the material

constitutive law is of primary importance for the accuracy of the subsequent numerical simulations of the implant. Moreover, the precise estimation of the material response up to large strain under different stress states is crucial to properly describe the evolution of ductile damage over the loading history, to assess the structural integrity of the prosthesis. Thus, the SLM Ti4Al4 alloy was tested under four different loading conditions, running the same number of tests on dedicated geometries. Namely, the selected tests were tensile tests on round bars (RB) and on round notched bars (RNB), tensile tests in plane strain condition (PS) and torsion tests on round bars. The corresponding specimen geometries are reported in the following Figure 1.
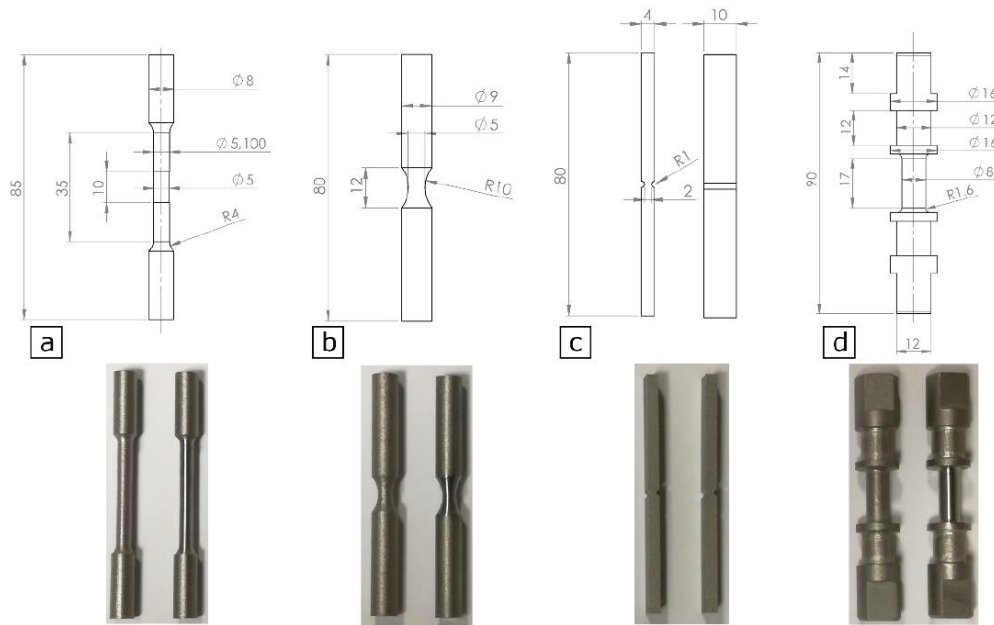
Figure. 1 Technical drawings and actual pictures of SLM Ti6Al4V: a) RB, b) RNB, c) PS d) torsion. All the dimensions are in mm.

From tensile tests on round bars the material constitutive engineering stress – strain curve was retrieved as shown in Figure 2A. Subsequently, the constitutive law was extended up to large strain using numerical inverse methods relying on the use of FEA, also. The resulting stress – strain curve is presented in Figure 2B and its analytical formulation reported in Equation 1.

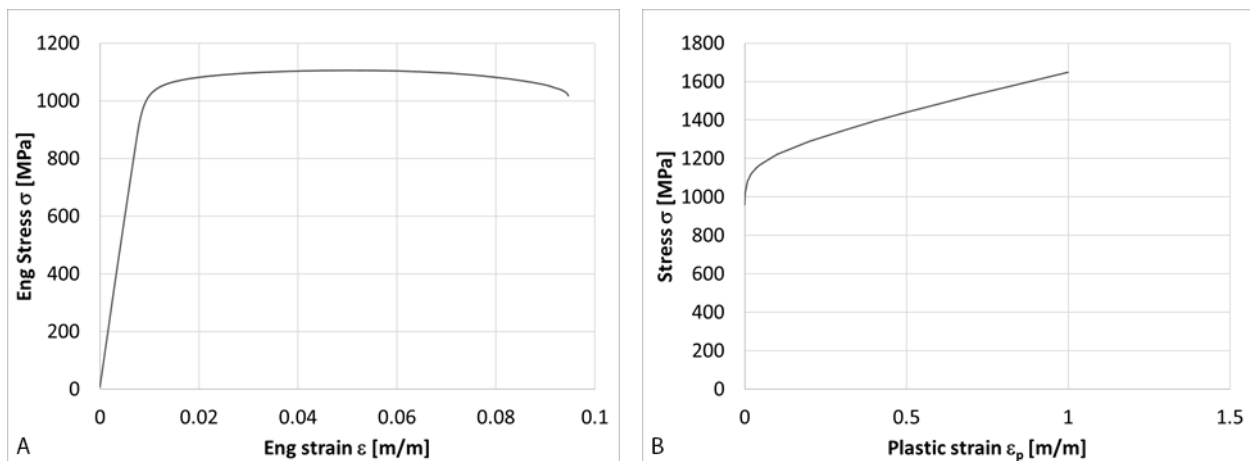$$\sigma = 1420\varepsilon^{0.08} + 200\varepsilon \tag{1}$$

Figure. 2 (A) Engineering stress-strain curve evaluated from tensile tests on RB samples; (B) Constitutive law retrieved up to large strain.

Taking advantage of this previous experimentation, in this study a ductile damage model was used to predict the plastic collapse and failure limits of the prosthesis in case of overload, allowing to lighten the prosthesis in the design phase without compromising safety with respect to structural integrity.

Design of the hip prosthesis implant and modelling of the human femur

Different CAD models of prospective femoral stem implants were designed based on different shapes, taken from literature studies or commercially available already. More specifically, three different external geometries were considered: (1) single wedge; (2) single wedge with collar; (3) single anatomical wedge. More details about the three different femoral implants are summarized in Table 3. As shown in Figure 3, for all implant designs the femoral stem axis was aligned with z-axis of the global coordinate system pointing upward, the x-axis is pointing toward the centre of pelvis, and the y-axis oriented consequently according to right-handed system.

Table 3. Classification of cementless femoral stem designs: type, geometry and description.

| Type	Geometry	Description
1	Single wedge	In the frontal plane, the design is one-half proximal flat in the anterior-posterior direction ending with a spherical distal edge. Medially, it presents a neck-shaft angle of 130°, vertically shaped in the lateral portion of the sagittal plane.
2	Single wedge with collar	In addition to the geometry of type 1, the type 2 sports a proximal collar with a prominent semi-circular disc shape in the medial portion of the sagittal plane. The collar is aimed to enhance the implant stability and favouring axial forces transmission from the femoral implant to the femoral bone metaphysis.
3	Single anatomical wedge	In type 3, a deeper curvature starts from the neck to a ninth of proximal stem edge and a narrow wedge is made in the proximal part to promote compression forces transmission on the femoral bone metaphysis.
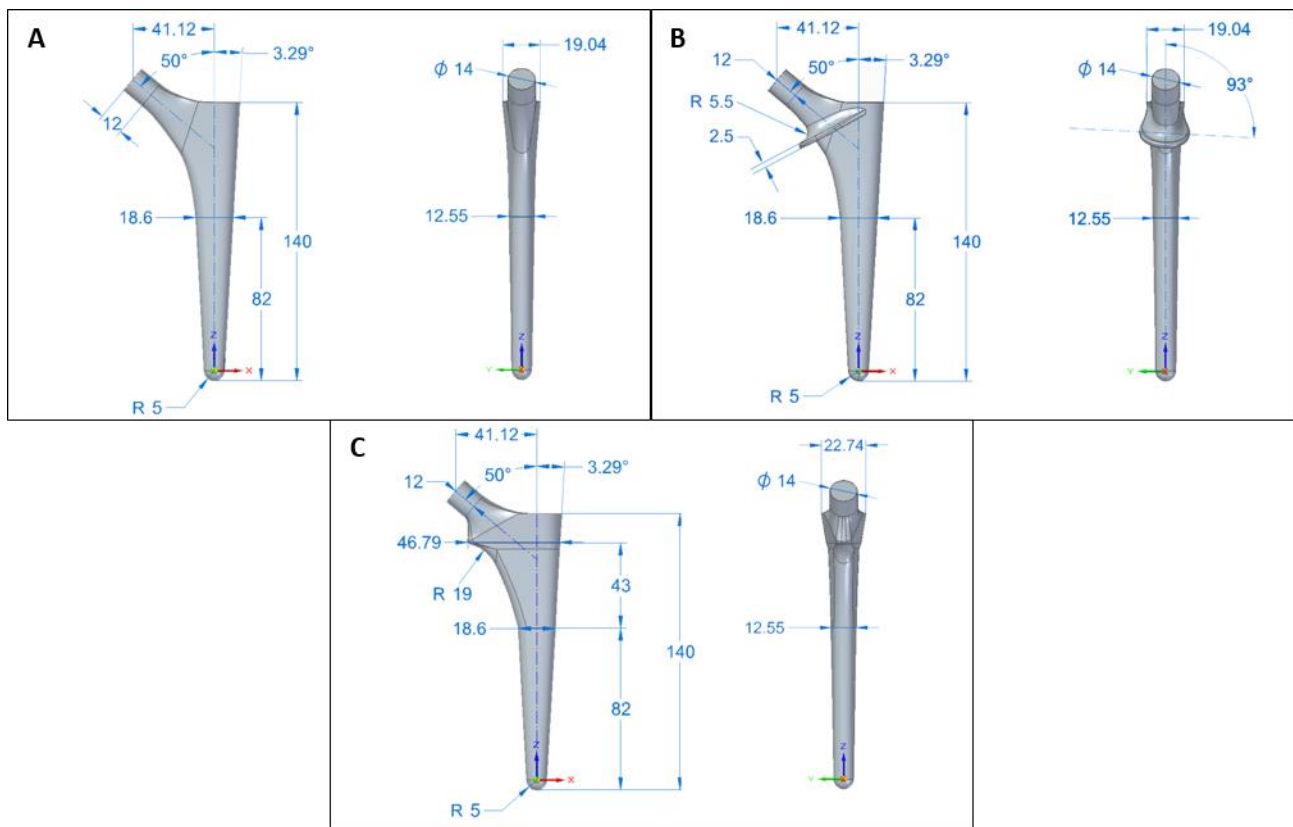
Figure 3. Lateral and frontal views of CAD models of femoral stem implants: (A) type 1 implant; (B) type 2 implant; (C) type 3 implant. Dimensions are expressed in mm.

The femoral head was modelled with a diameter of 32 mm and applied to the proximal implant neck. The femoral structure of the bone was designed in a CAD software according to a real CT-scan of a human subject and then imported in the Design Modeler of Ansys Workbench software. Taking into account the real morphology of a human femur, the model of the femoral bone was divided into three regions, as reported in Kharmanda et al. [20]: (i) internal metaphysis and epiphysis portion of both proximal and distal edge for the trabecular bone; (ii) internal medial diaphysis for the bone marrow; (iii) external layer for the cortical bone. The cortical layer was designed with 10 mm of maximum width in the half of the femur and 11.4 mm in the distal part, while the minimum width was 3 mm and 3.4 mm in the proximal and in the distal epiphysis, respectively. This subdivision was aimed at differentiating the internal bone structures to attribute the proper mechanical properties in the finite element model. A schematic of the femoral inner subdivisions is reported in Figure 4. The femoral neck osteotomy angle was set to 28° from the femoral anatomical axis according to [21], as shown in Figure 4B. The femoral stem implant was rotated of 3° along with the x-axis to match femoral anatomical axis to the femoral stem axis.
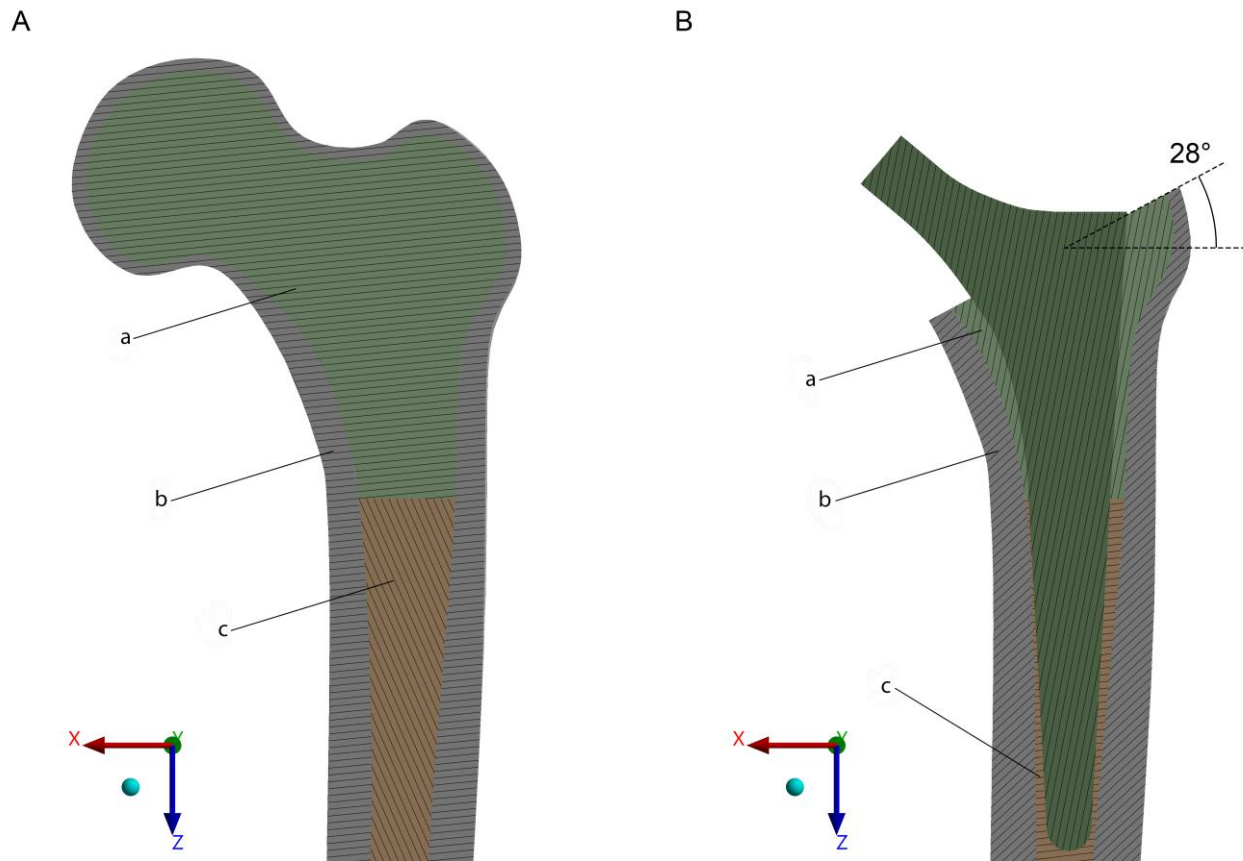

Figure 4. Lateral section of the human femoral CAD model. In A) the three region subdivisions are shown: (a) trabecular bone; (b) cortical bone; (c) bone marrow. In B) the stem implanted in the femur and osteotomy angle are reported.

The stem of the prosthesis, independently from the selected geometry, was modelled with an external solid skin and an inner reticular structure. A body centred cubic (BCC) type lattice structure was adopted allowing the parametrization of cell parameters, such as the lattice constant (l), the thickness of the inner trabeculae (s), and the fillet radius between cells (r), see Figure 5. Among other lattice structures, the BCC presents a higher maximum compressive stress and lower overall stiffness [22]. The external solid skin had a thickness ranging from 1 mm to a maximum of 7.5 mm in the proximal edge, see again Figure 4. For all femoral stem types described in Table 3, different equivalent densities were numerically tested. The most promising ones were 18.5% and 5% of equivalent density. For the sake of conciseness, only the results about the lighter one (5%) were presented and discussed in the following. For reference, a standard full dense configuration was simulated for each geometry, also. In Table 4, all implant configurations are summarized.
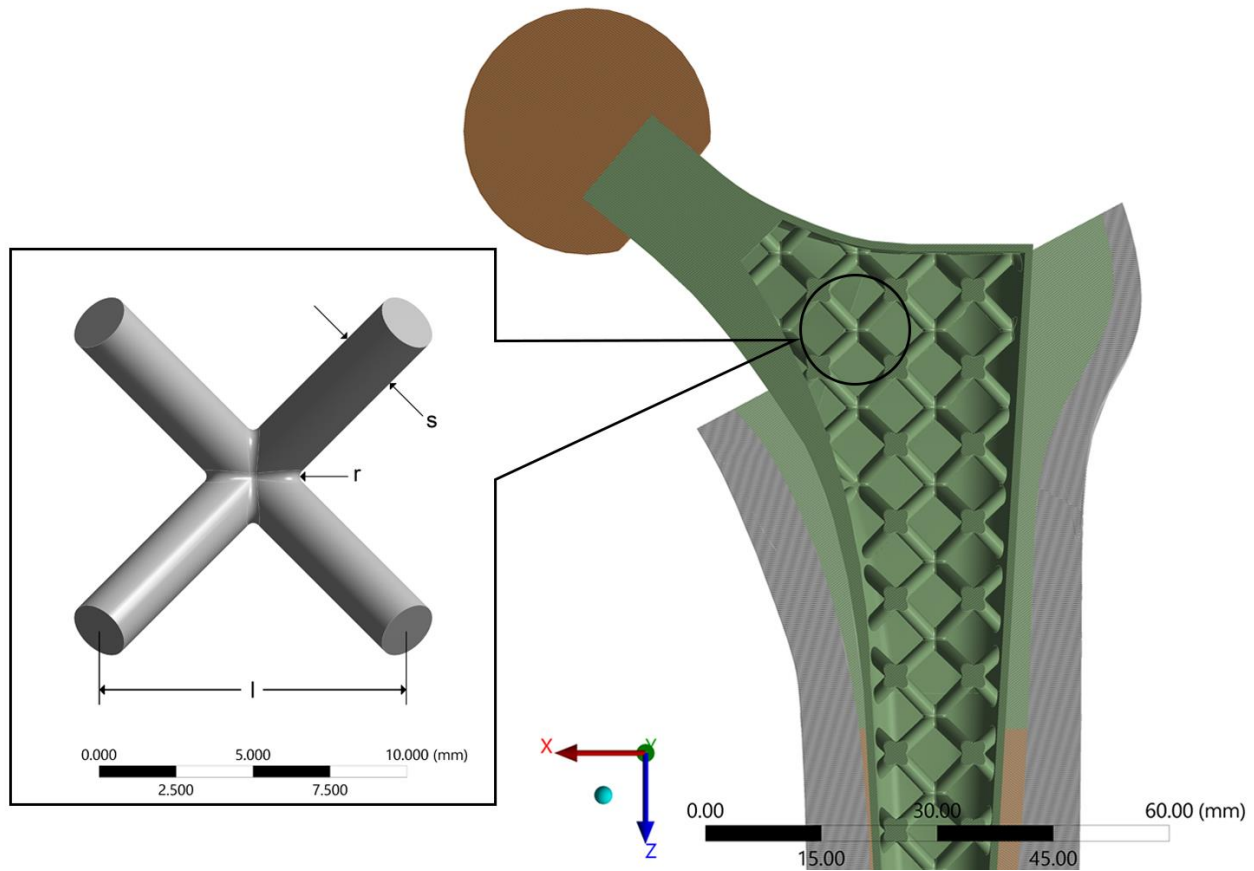
Figure 5. Section view of the overall system showing the lighter femoral stem and a focus on the lattice structure.

Table 4. Configurations of the different femoral stem implants tested. Name type, cell parameters, internal density and volume, weight and mass reduction with respect to the bulky implant were reported.

Type	Name	s (mm)	Density (%)	Volume (mm^2)	Weight (g)	Mass reduction (%)
1	1a	.	100	33100	146.3	-
	1b	1	5	12700	56.3	61.5
2	2a	.	100	33100	146.3	-
	2b	1	5	12700	56.3	61.5
3	3a	.	100	37200	164.5	.
	3b	1	5	12800	56.5	65.6

Finite Element model of the implant

The finite element model of the hip prosthesis implant consists in an assembly of the solid model of the femur and the prosthesis. In the different simulated scenarios, for each geometry two FE models of the prosthesis were analysed: a bulky one (full density 100%) and another with an inner trabecular structure with an equivalent density of 5%. An additional finite element analysis was also setup modelling a healthy femur alone, to be compared with the previous models to quantify the stress-shielding phenomenon.

The modelling of the femur with the hip prosthesis inserted was simplified by considering a unique value of the Young modulus for the whole proximal trabecular zone, equal to 200 [MPa], and 386 [MPa] for the entire distal trabecular zone. Instead, for the model of the healthy femur it was adopted a single value for the trabecular tissue equal to 386 [MPa]. The implant, that is to say the stem and the head of prosthesis, were regarded as made of SLM Ti6Al4V in as built conditions and Co-Cr-Mo alloy [20], respectively. Furthermore, all the materials in the FE model were considered as isotropic with the mechanical elastic properties summarized in Table 5.

Table 5. Material elastic properties used in the FE models

Material	Young's Modulus [MPa]	Poisson	Ref.
Cortical bone	18000	0.4	[23]
Proximal Trabecular bone	200	0.33	
Distal Trabecular bone	386	0.33	
Entire Trabecular bone (Healthy femur)	386	0.33	[20]
Bone marrow	3	0.25	
Co-Cr-Mo	230000	0.3	
Ti6Al4V	110000	0.3	

The connection between the outer part, i.e. cortical bone, and the inner part, i.e. trabecular bone plus bone marrow, was modelled as a bonded contact. The contact between femur and implant was set up as frictional, with a friction coefficient $f = 0.3$ as suggested by Sakai et al. [24]. All the FE models were meshed using tetrahedral and hexahedral elements with quadratic formulation. The average element dimensions range from 10 mm to 3.5 mm according to the meshed region. As an example, a section of the meshed femur with the implanted standard full prosthesis is reported in Figure 6.
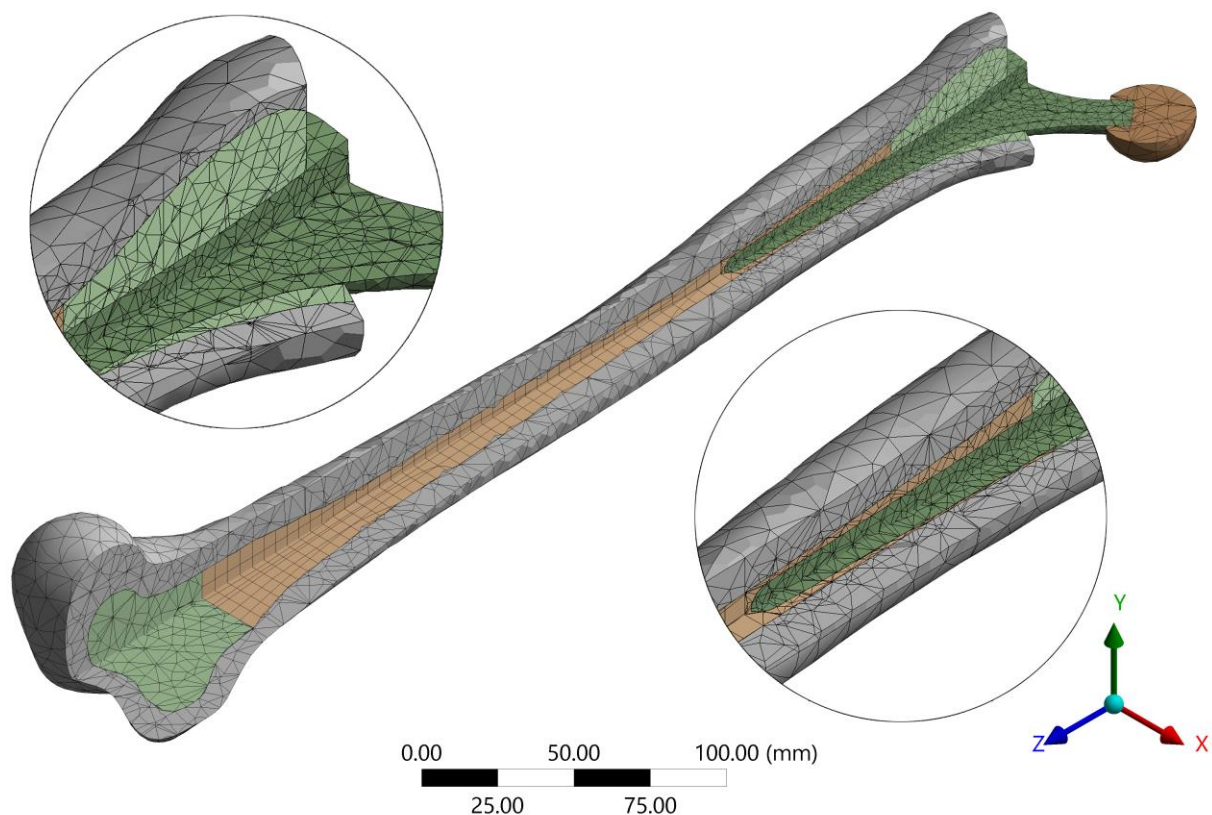

Figure 6. Meshed bulky hip prosthesis and human femur with subdivision in trabecular, cortical and bone marrow.

Load cases: Walking, stumbling and insertion

In the finite element analysis four different load cases were chosen: a first one to analyse the stress-shielding phenomenon, a second and a third one to assess the structural integrity of the prosthesis in case of accidental overloads and a final one reproducing a loading scenario in which the prosthesis was pushed up to plastic collapse. To study the first scenario a daily activity such as walking was considered. In the second scenario, an accidental event characterized by a high load, such as stumbling, was examined. For the third scenario an attempt was made to recreate the loading conditions that occur during the

surgical insertion of the prosthesis into the femur, by means of a surgery hammer stroke. Eventually, in the fourth case the load was increased up to the onset of plastic collapse. In the first two cases, the choice of the loads was made by referring to an online database in which data were collected from in vivo experimental activities carried out on patients with prostheses instrumented for the measurement of actual loads at the joints [25]. The data in the database are normalized in percentage to body weight (%BW - Body Weight). In these two scenarios a subject with a mass of 100 Kg was considered. The reference system used for the loads was chosen as follow: the origin is at the centre of the femoral head, i.e. the centre of the prosthesis head, the Z axis is towards to the midpoint of the two femoral epicondyles, the Y axis is directed laterally and consequently the X axis is directed anteriorly, see Figure 7a.

For walking, the maximum value of the force reached is 337 %BW, i.e. 3300 N, and its direction is exclusively along the Z axis. For stumbling, the maximum value of the force is 870 %BW, thus 8700 N. In this scenario a safety factor of 1.25 was chosen to further increase the load, reaching the force of 11000 N. This value was considered adequate to verify the structural integrity of the implant. Also in this case the direction of the force was chosen as that of the walk according to Bergmann et al. [26] i.e. the entire load was applied only along Z axis. Additionally, the force was increased until achieving the incipient rupture that was predicted thanks to the implementation of a ductile damage model in order to define the collapse safety factor. As already mentioned, for the walking scenario, a FE analysis of a healthy femur was carried out for comparison.

In the first two scenarios, the load was applied as a concentrated static force in the centre of the spherical head, while the displacement of the nodes belonging to the intercondylar fossa was prescribed, realizing a fixed support. In Figure 7b, an exemplificative scheme of the applied loads and constraints is shown.

For the third scenario, an attempt to reproduce the loading condition during surgery was carried out. To insert the stem, a surgical rasp is used to create a cavity inside the femur having the same shape as the chosen prosthesis, but smaller in size to create the mechanical interference required for press-fit fixation. Several authors reported that the force required to insert the stem into the cavity, measured using instrumented hammers, is equal to a maximum value of about 10 kN [24], [27]. This value was chosen as the limit value because it is the measured force needed to insert the stem into the cavity, and it has been demonstrated that for this value micro-fractures start to occur on the proximal femur according to [24] and [27].

In this case, a displacement was applied instead of a force to ensure the total insertion of the stem into the cavity and help the convergence of the FE solver. The prosthesis was placed above the cavity and concentric respect it, as reported in Figure 7C.
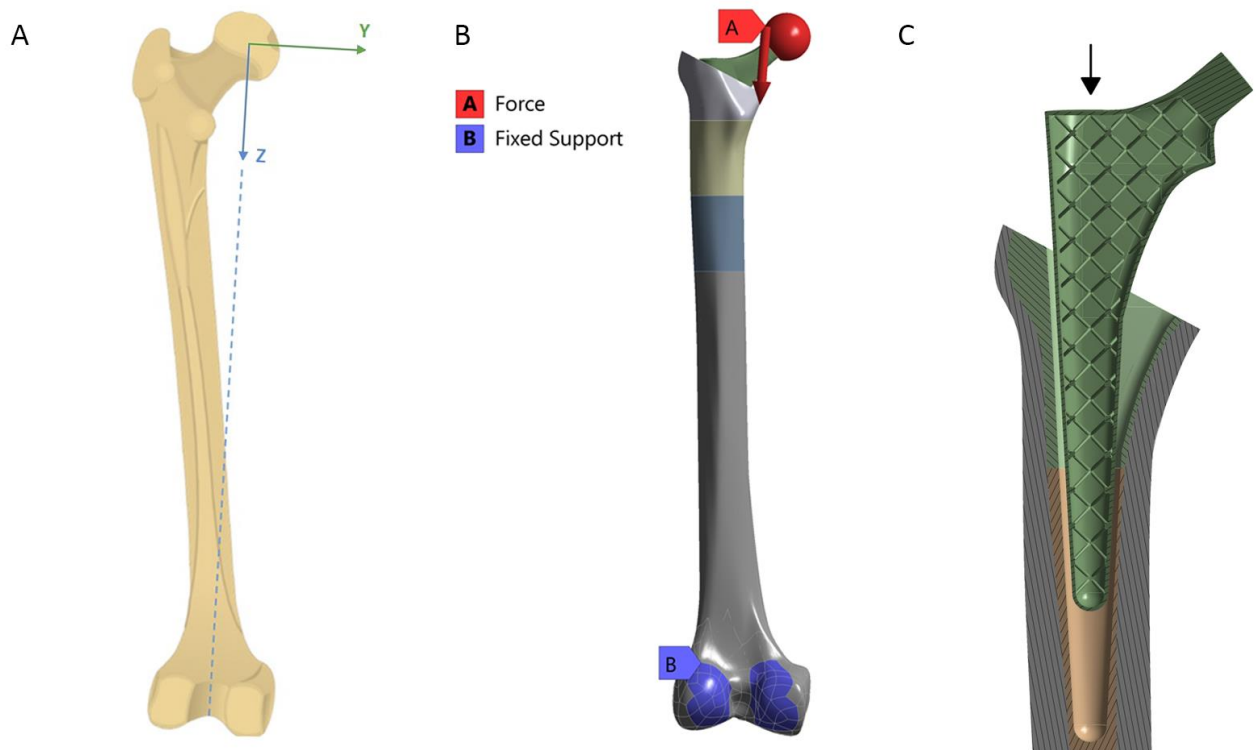

Figure 7. Representation of load cases: (A) human femur and reference system for the load applications (B) applied constraints in the case of walking scenario; (C) schematics of the insertion case.

The direction of displacement is parallel to the longitudinal axis of the cavity, again parallel to Z axis of the global reference system. The magnitude of the displacement was set equal to 37 mm: this value is small enough to minimize the calculation time, but large enough to avoid the initial contact between the implant and the femur to facilitate the convergence of the solution.

To the best of author's knowledge, in literature the value of the interference is not available, thus, a parametric adjustment of the interference was carried out as follows: the friction coefficient was fixed at 0.3, a displacement value was fixed also, and by varying the size of cavity the value of mechanical interference was obtained when the reaction force reached 10 kN. Several simulations were run, till a reaction force of 10kN was reached for an interference value of 0.36 mm. In this case, the distal femur region was regarded as fixed.

For the walking and stumbling cases, static structural analyses were carried out, while for the insertion a transient analysis was chosen to mitigate convergence issues during solution, caused by the initial lability between the prosthesis and the femur. Additionally, the displacement was applied in a long time span to make the inertial contribution of the bodies irrelevant.

Eventually, the fourth scenario was similar to walking and stumbling but the maximum force was not set a priori, but the load was increased up to the onset of the first plastic failure.

All the analysed load cases are summarized in Table 6.

Table 6. Summary or the studied load cases

Scenario	Purpose	Load/Displacement Value	Load/Displacement Direction	Constraint	Analysis type
Walking	Stress-shielding	3300 N	Axis Z		Static
Stumbling	Yield Strength	11000 N	Axis Z	Fixed support on distal femur	Static
Insertion	Yield Strength	37 mm	Parallel to axis of cavity		Transient
Plastic collapse	Ultimate Strength	Until rupture onset	Axis Z		Static

Structural integrity assessment

A ductile damage model was adopted in the present study to predict the plastic failure of the prosthesis in case of overload. Among the different ductile damage models available in literature, the one proposed by Coppola, Cortese and Folgarait was selected [28]. The accumulated ductile damage is quantified by a scalar parameter D that increases with the plastic strain increment weighted on a proper function of the stress state (Eq. 2). The stress state is expressed using one or two parameters: the stress triaxiality T and the Lode parameter X, which in turn depends on the invariants of the stress and deviatoric tensors as defined by Eq. 3 and 4 (for a more comprehensive theoretical background please refer to [29]).

$$D = \int_0^{\varepsilon_f} f(T,X)d\varepsilon_p \tag{2}$$

$$T = \frac{1}{3}\frac{I_1}{\sqrt{3J_2}} \tag{3}$$

$$X = \frac{27}{2}\frac{J_3}{(\sqrt{3J_2})^3} \tag{4}$$

I_1 is the first stress invariant, J_2 and J_3 the second and third deviatoric stress invariants.

Failure occurs when D reaches a critical value, conventionally set to unity. Under the assumption of proportional loading conditions, posing $D = 1$, Eq. 2 can be inverted resulting in a 3D surface in the three-dimensional space [T, X, ε_f] (Eq. 5), called fracture surface or fracture locus, for which a unique strain at fracture can be associated to each stress state.

$$\varepsilon_f = f^{-1}(T,X) \tag{5}$$

The fracture surface of the model proposed by Coppola, Cortese and Folgarait can be written as follows (Eq. 6):

$$\varepsilon_f = \frac{1}{C_1} e^{-C_2 T} \left(\frac{1}{\cos\left[\beta\frac{\pi}{6} - \frac{1}{3}\arccos(\gamma X) \right]} \right)^{\frac{1}{n}} \tag{6}$$

Where n is the hardening exponent, C_1, C_2, β and γ are four material parameters to be tuned. Testing the four different specimen geometries the Eq.6 permits the identification of the four experimental points in the T, X, ε_p space. The measured values are summarized in Table 7.

Table 7. Ti6Al4V: T, X and ε_p experimental values of the four calibration points

Ti6Al4V	T	X	ε_p
RB	0.42	1.00	0.31
RNB10	0.70	1.00	0.19
PS	0.61	0.29	0.05
Torsion	0.00	0.00	0.11

The calibration procedure consists in a minimization between the experimentally measured strain at fracture and the one predicted by the model for each different stress state. Eventually, the tuned fracture surface is reported in the following Figure 8, with the four calibration points marked as blue dots. In Table 8 the parameters calibrated in [16] are summarized.
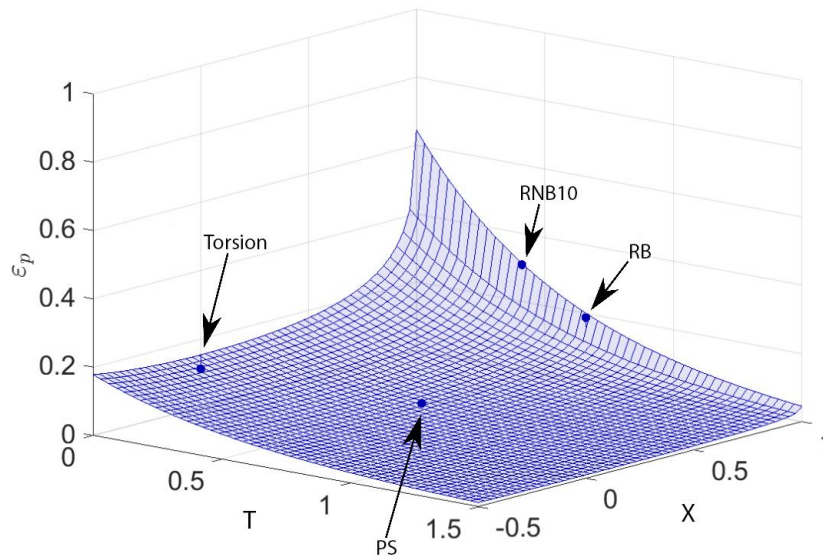

Figure 8. SLM Ti6Al4V: Fracture surfaces calibrated for the Coppola, Cortese and Folgarait model. The blue dots represent the experimental calibration points [16].

Table 8. Ti6Al4V: Calibrated parameters of the selected damage model

Ti6Al4V	C_1	C_2	β	γ
As Built	1.56	1.77	1.00	1.00

The tuned ductile damage model was embedded in the FE analysis via custom subroutine and profitable used to predict the initial fracture of the prosthesis.

To this purpose, a "Command" module was used in the pre-processor of Ansys Mechanical, to implement the model through a custom APDL script. The load was applied in multiple load steps and the script works with a recursive logic in every load step (LS) as follows: at each LS the stress state is computed and stored. For each element the averaged values over time of T and X are calculated (T_{av} and X_{av}) and stored themselves so that at each stage T_{av} and X_{av} are updated taking into account also T and X of the actual stage. Then, for each element the accumulated ductile damage D is computed relying on T_{av} and X_{av}. If, at any stage, the accumulated ductile damage overcomes the unity threshold ($D\geq 1$), the element is deactivated through the command "Ekill". The deactivated element remains in the model but contributes a near-zero stiffness value, namely its load bearing capacity becomes negligible. Moreover, graphically, the solver makes the element invisible to visually simulate a real failure. The deactivated elements IDs are transmitted to the next load steps in order to consider the absence of the elements with $D\geq 1$.
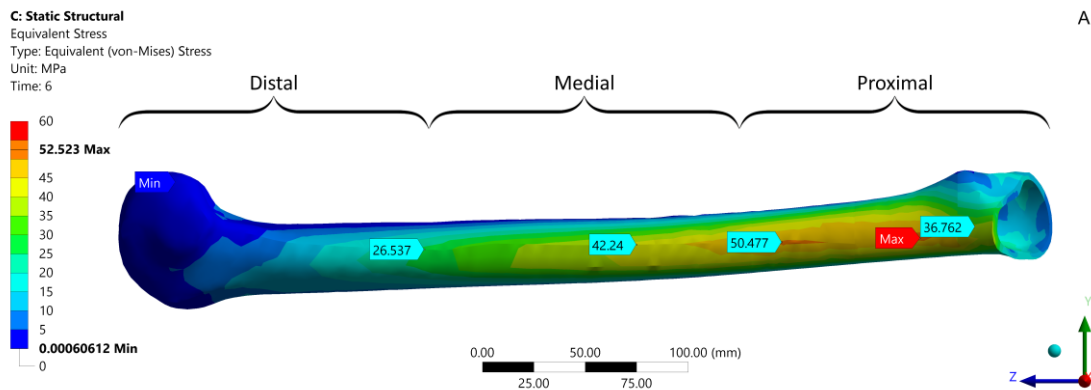
To plot the contour map of the accumulated ductile damage stage by stage, a second custom APDL script is adopted in the post-processing phase. The logic of this routine is the same as of the previous, with the difference that the elements are not deactivated and the values of D of each element are stored at each stage.

An example of "killed" elements and of the damage contour map were reported in Figures 16 and 17of the next section.

Results and Discussion

At first, the performance of the different types of prostheses in re-establishing physiological load levels on the bone will be presented. Afterwards, the results to assess the structural integrity of the most promising implant will be shown.

In Figure 9 it is reported a comparison of the equivalent Von Mises stress on cortical bone only in the three cases of: healthy femur, bulk prosthesis with single wedge design (type 1a in Table 3) and in the case of anatomical wedge prosthesis with an equivalent density of 5% (type 3b in Table 3).
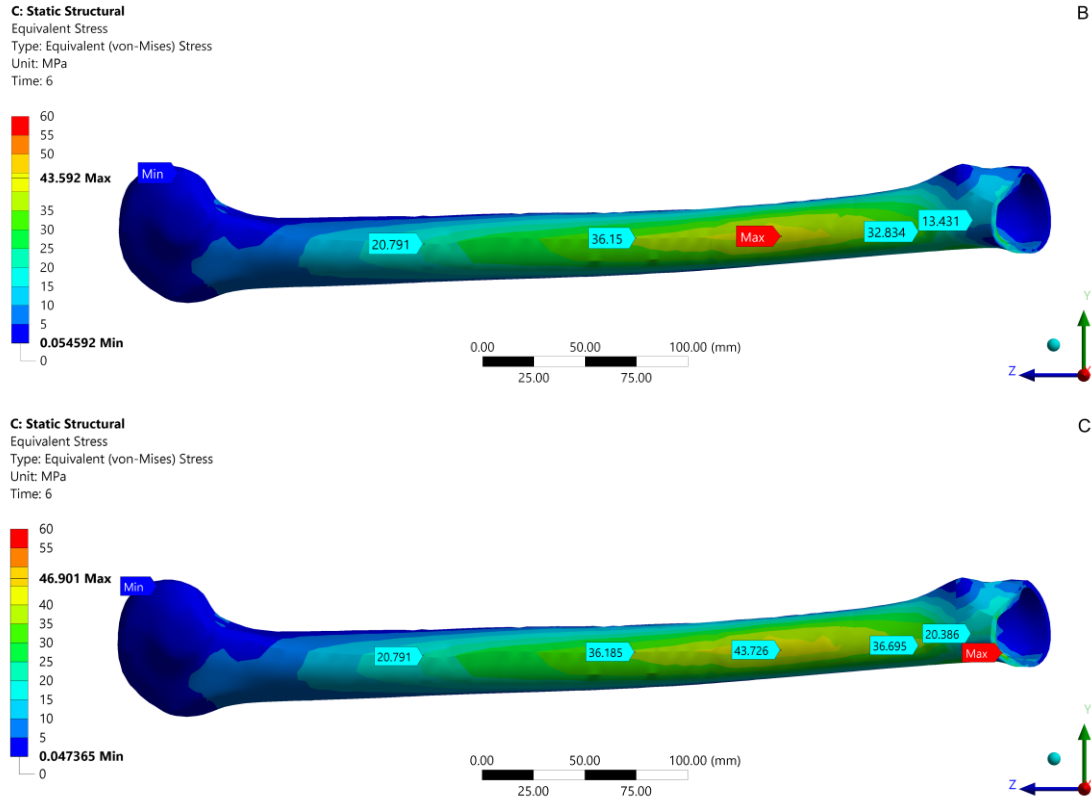
C: Static Structural
Equivalent Stress
Type: Equivalent (von-Mises) Stress
Unit: MPa
Time: 6

B

C: Static Structural
Equivalent Stress
Type: Equivalent (von-Mises) Stress
Unit: MPa
Time: 6

C

Figure 9. Comparison between: (A) case of healthy femur; (B) case of implanted femur in full dense prosthesis with single wedge; (C) case of implanted femur with prosthesis with single anatomical wedge with an equivalent density of 5%

As expected, where the implant is present, the contour map revealed a marked drop of the stress level in the whole proximal region; in addition, the maximum VM stress value decreases from 52 MPa to 43 MPa and shifts towards the diaphysis of the femur, leaving the proximal area more unloaded. In the literature [10], the Gruen Zone 7 (GZ7) and 6 (GZ6) can be considered the most affected regions by the stress shielding. Therefore, a set of critical nodes were selected in these two areas as shown in Figure 10 and Figure 11. Thanks to the use of an identical mesh for each simulation, it was possible to examine the same spot for all results. The stress shielding can be evaluated using the following formula (Eq. 7), suggested by Alkhatib et al. [30],

$$Stress\ shielding = \frac{Y_{imp} - Y_{ref}}{Y_{ref}} \tag{7}$$

where Y_{ref} and Y_{imp} are the equivalent Von Mises stress of the healthy and implanted femur respectively. In the case of a decrease of stress in the bone, the result is negative. Instead, if the bone is overloaded the result is positive. Thus, the goal of this study is to increase these values and ideally make them equal to zero, which means no stress-shielding effect and a physiological load on the bone.

For the sake of the completeness, Figures 10 and 11 report the stress shielding value in percentage for all the types of prostheses previously described.
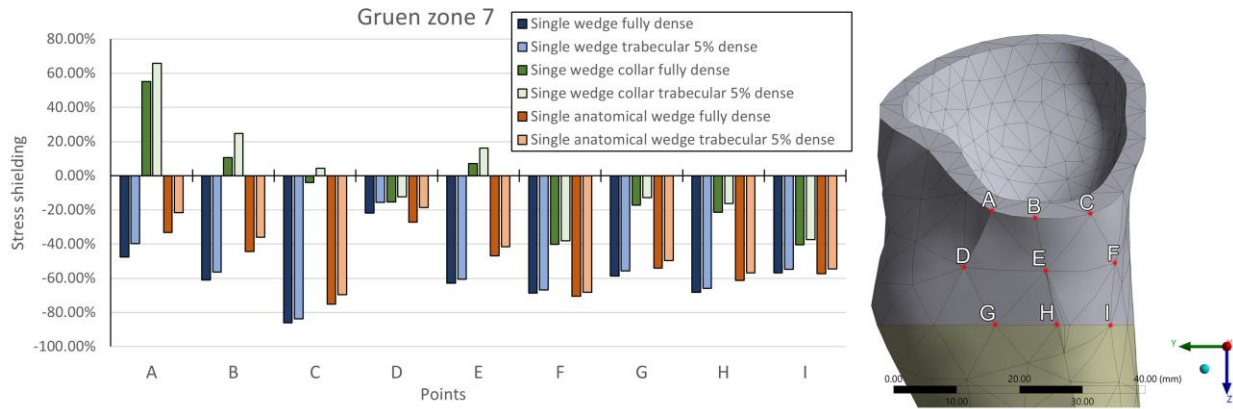
Figure 10. Value of stress shielding in the Gruen zone 7 for all considered prosthesis types
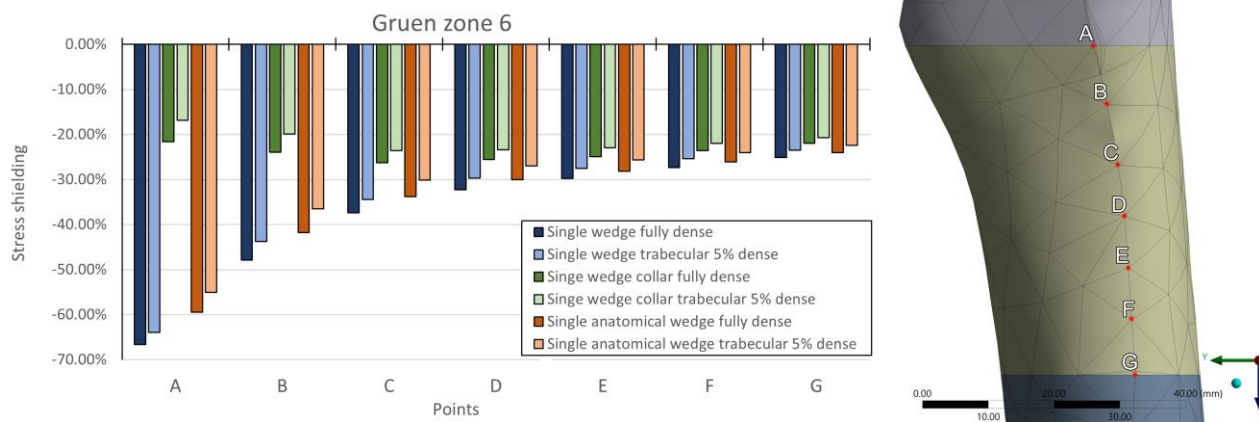

Figure 11. Value of stress shielding in the Gruen zone 6 for all considered prosthesis types

Then, regarding the bulk prostheses, independently from the external geometry, it is evident that the addition of the collar and the anatomical configuration are both beneficial for the femur increasing the level of stress on GZ7 and GZ6. In some nodes belonging to the configuration of the prosthesis with collar (type 2a Table 3) it is even present an overload. Moreover, the internal trabecular structure allows a further intensification of the reduction of the stress shielding. This result is important because, in addition to trying to re-establish the physiological loads on the femur, it shows how the use of a trabecular structure has general validity regardless of the geometry and shape of the chosen prosthesis.

From a merely numerical point of view, the trabecular configuration with collar (type 2b Table 3) seemed to show a greater reduction of stress shielding with respect to the others, but was not regarded as the best solution due to some negative aspects. In fact, the overload induced by direct contact between the collar and the femur could have side negative impacts on the bone. In addition, the direct contact could lead to impulsive forces that the surgeon might transfer with the hammer trough the implant, damaging the already fragile bone surface. Furthermore, another negative aspect may concern a possible imperfect contact between the surface of the femur and the surface of the collar caused by a mismatch of the angle of inclination of the collar in respect with that of the surface of the bone subjected to surgical cut. This mismatch can result from a manufacturing error or an incorrect cut by the surgeon. For the reasons expressed above, among all the versions of prostheses analysed, as the most effective it was finally selected the one with single anatomical wedge with internal trabecular structure with an equivalent density of 5% (type 3b Table 2). This configuration permitted to obtain a reduction of stress shielding up to 11% and 25% in GZ6 e GZ7, respectively. Table 9 reports the consistent load percentage increase, produced by the anatomical configuration compared to the type with single wedge fully dense, confirming the benefits of the chosen solution.

Table 9. Load variation (%) reported by the anatomical configuration dense at 5% with respect to the configuration of single wedge fully dense (%)

Area	A	B	C	D	E	F	G	H	I
GZ6	35	22	12	8	6	5	4		
GZ7	50	64	117	4	57	1	22	36	5

It should be noted that there is no linear correlation between stress shielding reduction and actual beneficial effects on the bone, meaning that even a reduction of a few percentage points could be important for the activation of those grow processes that balance those of bone resorption. The only direct evaluation that can be performed is the one carried out radiographically by means of osteodensiometry that evaluate bone mineral density.

Having selected the most promising design of the best prosthesis to diminish the stress shielding, the structural integrity had to be assessed in case of the worst common accidental event for the femur: the stumbling. A static load of 11000 N was applied along the Z axis. According to Figure 12, almost all the regions of the prosthesis were characterized by values of equivalent Von Mises stress below the yield strength of the material (959 MPa). Only in a small region, on the curved part of the prosthesis, the local stress slightly exceeded the yield point. However, considering the adjacent area to these regions, the average equivalent stress value is lower than 959 MPa, therefore them can be structurally considered as non-critical areas. Moreover, in Figure 13 the contour map of equivalent plastic strain is reported, exhibiting a maximum only of 1%, while the average value of the area subjected to plastic deformation is definitely below 1%. Furthermore, in this case, the load was applied statically, while in actual stumbling, the application of the load is impulsive, meaning that the simulated scenario was more critical than the real one. Additionally, as already mentioned, the applied force has been increased by a safety factor equal to 1.25. For all the considerations above, the model of single anatomical wedge 5% (type 3b in Table 3) can be considered as structurally safe.
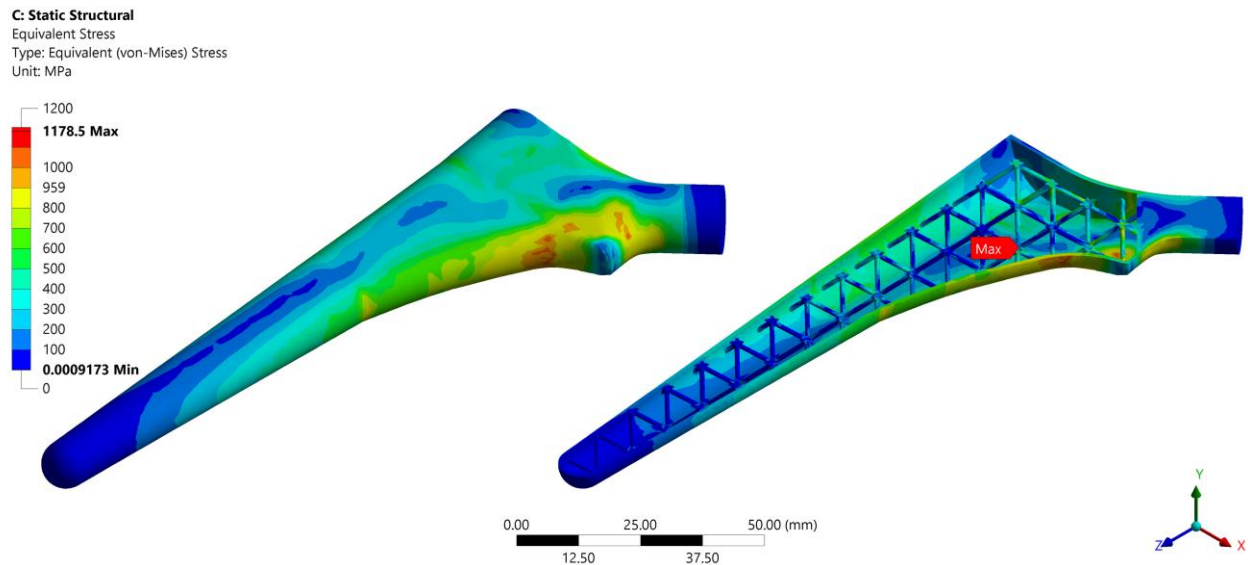

Figure 12. Contour map of equivalent Von Mises stress of the prosthesis with single anatomical wedge, with internal trabecular structure 5% dense, in the stumbling scenario.
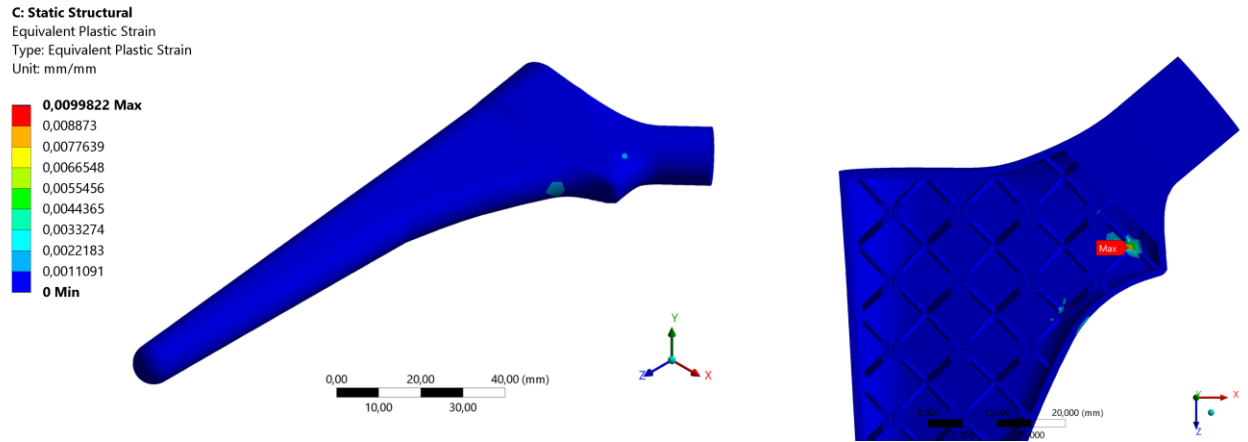
Figure 13. Contour map of the equivalent plastic strain of the prosthesis with single anatomical wedge, with internal trabecular structure 5% dense, in the stumbling scenario.

In the following Figures 14 and 15, the contour map of the equivalent Von Mises stress and the equivalent plastic strain on the prosthesis during the THA insertion are presented, respectively. The proximal zone of the prosthesis is the most stressed. The Von Mises stress exceeded the yield point of 50 MPa on average only on some trabeculae under the top surface. On the other hand, the rest of the prosthesis remained well below the yield point. A local peak of 1153 MPa is observed on one single node, which can therefore be considered negligible. Moreover, the equivalent plastic strain is marginal, being below 1%. It is important to notice that in the simulation the displacement was applied in one second unlike in reality where the hammering is impulsive, occurring in about 0.1ms [24]. Furthermore, in the model, the total energy necessary for the insertion of the prosthesis was provided in one stroke unlike what happens during surgery, where the surgeon distributes the energy in several strokes, gradually inserting the stem. For the reasons listed above, the outcome of the structural integrity of trabecular prosthesis during THA can generally be assumed to be confirmed.
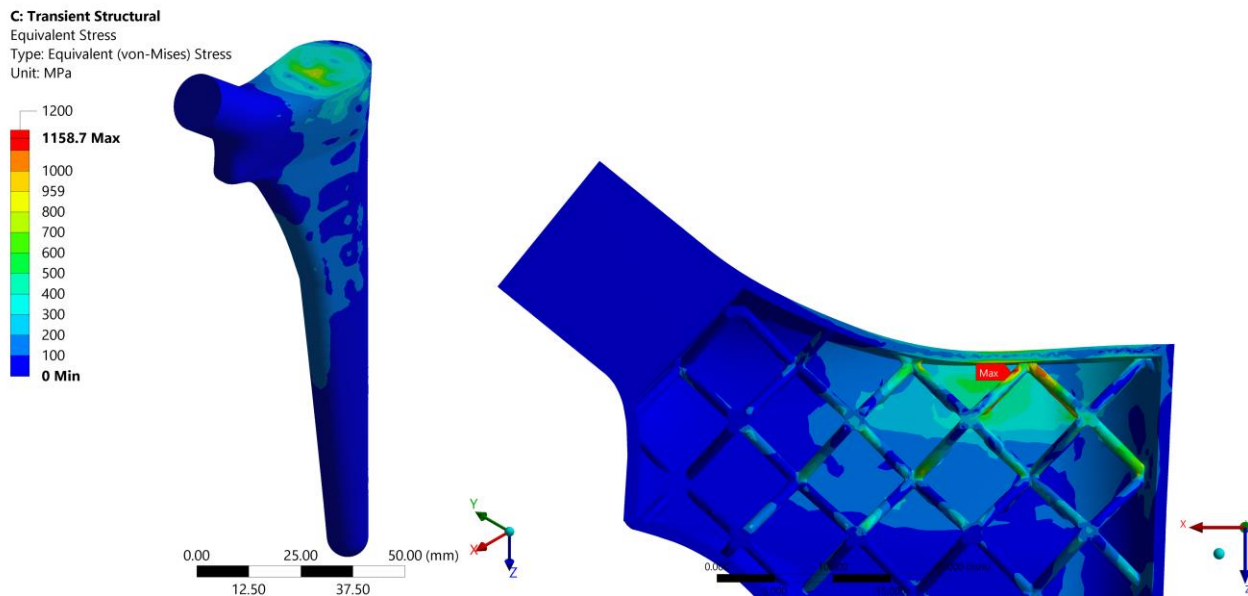

Figure 14. Contour map of equivalent Von Mises stress of the prosthesis with single anatomical wedge, with internal trabecular structure 5% dense, in the insertion scenario.
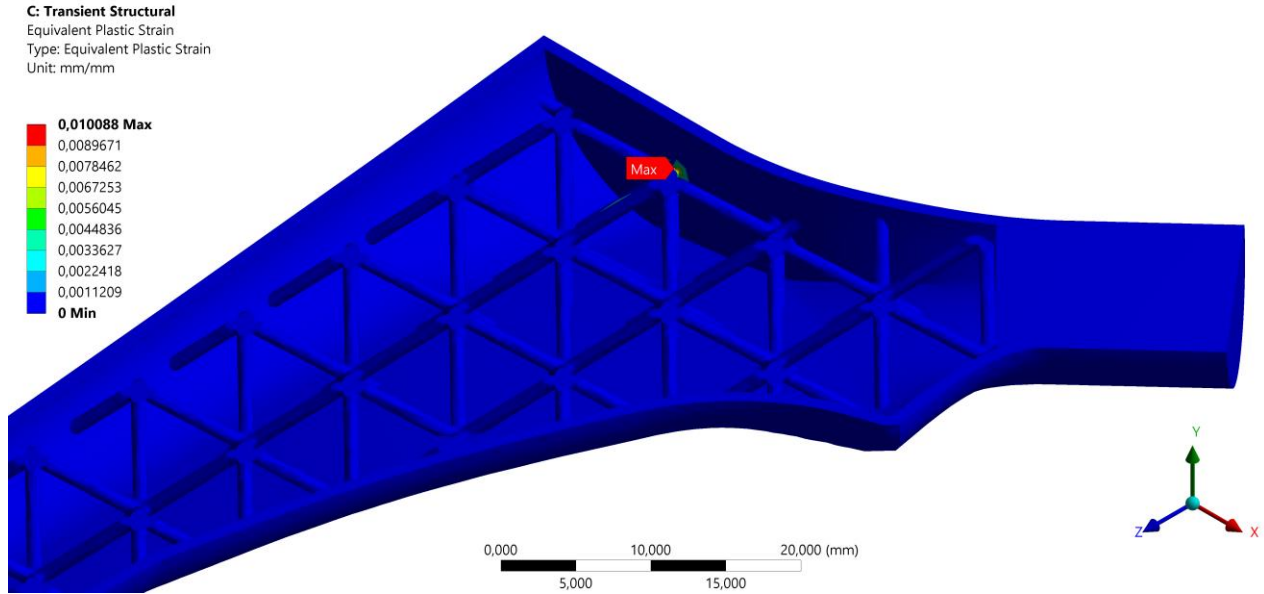
Figure 15. Contour map of the equivalent plastic strain of the prosthesis with single anatomical wedge, with internal trabecular structure 5% dense, in the insertion scenario.

The latest results to be discussed were those concerning the simulation of plastic collapse of the prosthesis, to evaluate the safety margin after the yield point up to failure. Figure 16A illustrates the first element killed: it is located inside the trabecular structure in the proximal area of the prosthesis. The damage indicator (*D*) of the element has reached the unit (*D=1*) for a considerable load value equal to 17820 N. Also, the Figure 16B exhibits the contour map of equivalent plastic deformation where the failure occurred for a strain value about of 0.13 mm/mm in the region of the killed element. This evidence suggests that the prosthesis with single anatomical wedge with a density of 5% (type 3b in Table 3) can be considered safe until a static load of 17820 N. Furthermore, referring to the stumbling simulation, in which the load was 11000 N, a safety factor on the maximum load at failure can be defined, being in this specific case about 1.6. The Figure 17A represents the contour map of damage indicator an instant before the plastic failure (*D = 0.97*), instead in Figure 17B and 17C the evolution of the damage indicator is shown, highlighting that the most critical parts of the prosthesis are the external surface and the internal trabeculae, both in the proximal region.
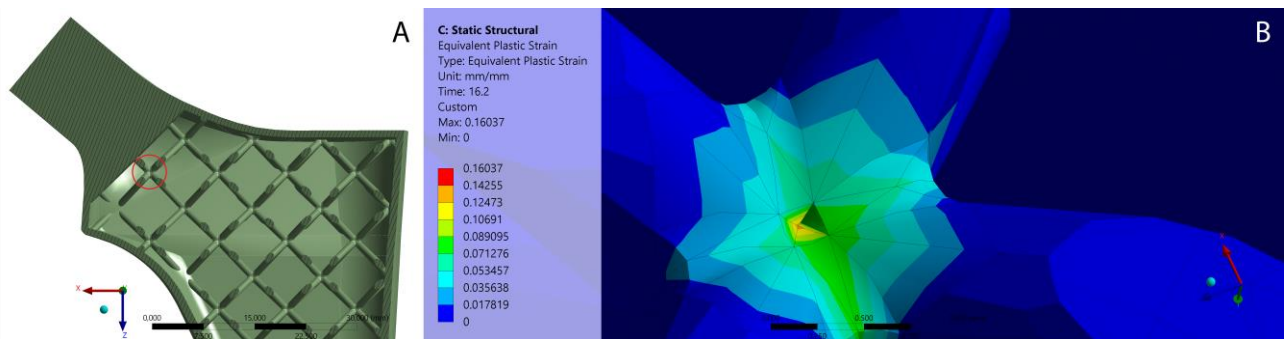

Figure 16. (A) The position of the killed element; (B) The contour map of the equivalent plastic strain in the region of the killed element
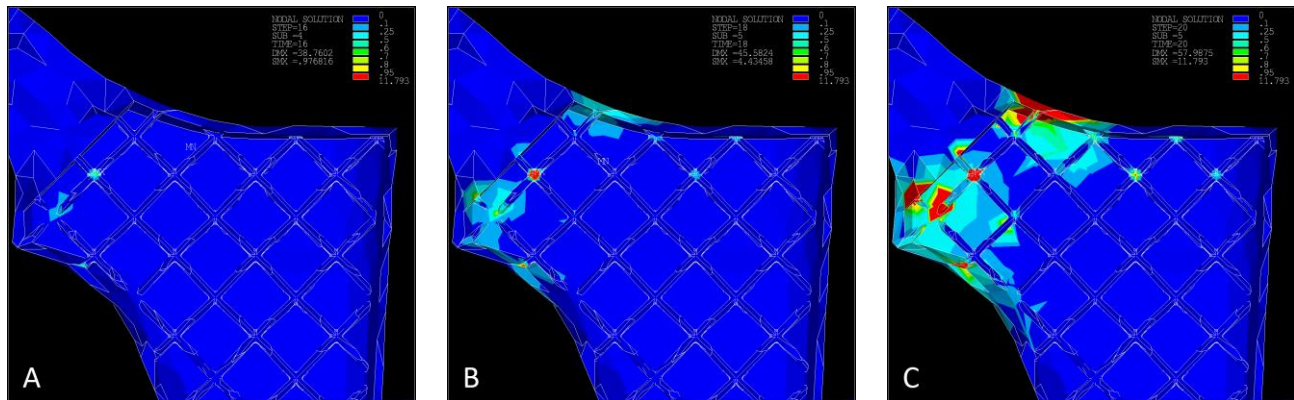
Figure 17. (A) Instant before the plastic failure, D = 0.97; (B and C) Evolution of the damage indicator D with progressive plastic deformation

Conclusions

Through an accurate study of a parametric FE model of the Ti6Al4V THA implant, it was demonstrated how the redesign of a conventional prosthesis taking advantage of AM technology allows to mitigate the stress shielding phenomenon and therefore to enhance the structure-bone integration.

The main findings can be summarized as follows:

- Regarding the bulk prosthesis, the addition of a collar or the use of anatomical configuration seem to be beneficial increasing the value of the stress in the proximal bone, i.e. in the GZ7 and GZ6.
- Taking advantage of AM technology, the internal trabecular structure allows a further reduction of the stress shielding regardless the geometry and the shape of the chosen prosthesis.
- Among the different types of prosthesis analysed, the best solution in terms of stress shielding was the single anatomical wedge with equivalent density of 5%.
- The assessment of the structural integrity under yield point was carried out by means of FE simulation of unconventional loading test such as the stumbling and the insertion during THA surgery.
- The identification of the failure load was performed by means of a damage model that predicts the onset of the plastic collapse of the material.

In the future, other possible geometries and shapes taking advantage of AM technology should be explored. Moreover, an experimental phase to assess the structural integrity of the chosen prosthesis should be carried out.

The results of this study are encouraging and might be validated through a clinical follow-up once a prosthesis with an internal trabecular structure, similar to the one described in this article, has been implanted to actual patients.

Declaration of Conflicting Interests

References

[1] I. D. Learmonth, C. Young, and C. Rorabeck, "The operation of the century: total hip replacement," *Lancet*, vol. 370, no. 9597. Lancet, pp. 1508–1519, Oct-2007.

[2] M. Sloan, A. Premkumar, and N. P. Sheth, "Projected volume of primary total joint arthroplasty in the u.s., 2014 to 2030," *J. Bone Jt. Surg. - Am. Vol.*, vol. 100, no. 17, pp. 1455–1460, 2018.

[3] R. Huiskes, H. Weinans, and B. Van Rietbergen, "The relationship between stress shielding and bone resorption around total hip stems and the effects of flexible materials," in *Clinical Orthopaedics and Related Research*, 1992, vol. 274, no. 274, pp. 124–134.

[4] M. I. Z. Ridzwan, S. Shuib, A. Y. Hassan, A. A. Shokri, and M. N. Mohammad Ibrahim, "Problem of stress shielding and improvement to the hip implant designs: A review," *Journal of Medical Sciences*, vol. 7, no. 3. Asian Network for Scientific Information, pp. 460–467, Apr-2007.

[5] H. S. Khanuja, J. J. Vakil, M. S. Goddard, and M. A. Mont, "Cementless femoral fixation in total hip arthroplasty," *Journal of Bone and Joint Surgery - Series A*, vol. 93, no. 5. Journal of Bone and Joint Surgery Inc., pp. 500–509, Mar-2011.

[6] M. Loppini and G. Grappiolo, "Uncemented short stems in primary total hip arthroplasty: The state of the art," *EFORT Open Rev.*, vol. 3, no. 5, pp. 149–159, May 2018.

[7] M. Moga and M. E. Pogarasteanu, "Technical considerations and functional results in primary uncemented hip arthroplasty using short femoral stems through mini-invasive techniques," *J. Med. Life*, vol. 7, no. 3, pp. 403–407, Sep. 2014.

[8] J. T. Kim and J. J. Yoo, "Implant Design in Cementless Hip Arthroplasty," *Hip Pelvis*, vol. 28, no. 2, p. 65, 2016.

[9] K. B. Hazlehurst, C. J. Wang, and M. Stanford, "A numerical investigation into the influence of the properties of cobalt chrome cellular structures on the load transfer to the periprosthetic femur following total hip arthroplasty," *Med. Eng. Phys.*, vol. 36, no. 4, pp. 458–466, Apr. 2014.

[10] S. Arabnejad, B. Johnston, M. Tanzer, and D. Pasini, "Fully porous 3D printed titanium femoral stem to reduce stress-shielding following total hip arthroplasty," *J. Orthop. Res.*, vol. 35, no. 8, pp. 1774–1783, 2017.

[11] D. Pasini, "Sajad Arabnejad Khanoki Multiscale Design and Multiobjective Optimization of Orthopedic Hip Implants with Functionally Graded Cellular Material," 2012.

[12] S. Arabnejad Khanoki and D. Pasini, "Fatigue design of a mechanically biocompatible lattice for a proof-of-concept femoral stem," *J. Mech. Behav. Biomed. Mater.*, vol. 22, pp. 65–83, Jun. 2013.

[13] R. Aversa, F. Ion, T. Petrescu, R. Victoria, V. Petrescu, and A. Apicella, "Flexible Stem Trabecular Prostheses," *Am. J. Eng. Appl. Sci. Orig. Res. Pap.*, 2016.

[14] Y. E. Delikanli and M. C. Kayacan, "Design, manufacture, and fatigue analysis of lightweight hip implants," *J. Appl. Biomater. Funct. Mater.*, vol. 17, no. 2, Apr. 2019.

[15] F. Nalli, A. D'Onofrio, G. B. Broggiato, and L. Cortese, "Calibration and prediction assessment of different ductile damage models on Ti6Al4V and 17-4PH additive manufactured alloys," in *Procedia Structural Integrity*, 2019, vol. 24, pp. 810–819.

[16] F. Nalli, L. Cortese, and F. Concli, "Ductile damage assessment of Ti6Al4V, 17-4PH and AlSi10Mg for additive manufacturing," *Eng. Fract. Mech.*, vol. 241, p. 107395, 2021.

[17] M. Windler and R. Klabunde, "Titanium for Hip and Knee Prostheses," in *Titanium in Medicine*, 2001, pp. 703–746.

[18] A. Schuh, J. Bigoney, W. Hönle, G. Zeiler, U. Holzwarth, and R. Forst, "Second generation (low modulus) titanium

alloys in total hip arthroplasty," *Materwiss. Werksttech.*, vol. 38, no. 12, pp. 1003–1007, 2007.

[19] EOS GmbH, "Titanium Ti6Al4V - Material Data Sheet," vol. 49, no. 0. pp. 1–5, 2014.

[20] G. Kharmanda and A. El Hami, *Biomechanics*, vol. 5. Hoboken, NJ, USA: John Wiley & Sons, Inc., 2016.

[21] D. Dimitriou, T. Y. Tsai, and Y. M. Kwon, "The effect of femoral neck osteotomy on femoral component position of a primary cementless total hip arthroplasty," *Int. Orthop.*, vol. 39, no. 12, pp. 2315–2321, Dec. 2015.

[22] A. Seharing, A. H. Azman, and S. Abdullah, "A review on integration of lightweight gradient lattice structures in additive manufacturing parts," *Adv. Mech. Eng.*, vol. 12, no. 6, p. 168781402091695, Jun. 2020.

[23] L. Cristofolini, M. Juszczyk, F. Taddei, and M. Viceconti, "Strain distribution in the proximal human femoral metaphysis," *Proc. Inst. Mech. Eng. Part H J. Eng. Med.*, vol. 223, no. 3, pp. 273–288, Apr. 2009.

[24] R. Sakai *et al.*, "Hammering force during cementless total hip arthroplasty and risk of microfracture," *HIP Int.*, vol. 21, no. 3, pp. 330–335, May 2011.

[25] P. Damm and A. Bender, "Orthoload." [Online]. Available: https://orthoload.com/.

[26] G. Bergmann, F. Graichen, and A. Rohlmann, "Hip joint contact forces during stumbling," *Langenbeck's Arch. Surg.*, vol. 389, no. 1, pp. 53–59, 2004.

[27] P. Pétursson *et al.*, "Bone mineral density and fracture risk assessment to optimize prosthesis selection in total hip replacement," *Comput. Math. Methods Med.*, vol. 2015, 2015.

[28] T. Coppola, L. Cortese, and P. Folgarait, "The effect of stress invariants on ductile fracture limit in steels," *Eng. Fract. Mech.*, vol. 76, no. 9, pp. 1288–1302, 2009.

[29] Y. Bai and T. Wierzbicki, "Application of extended Mohr-Coulomb criterion to ductile fracture," *Int. J. Fract.*, vol. 161, no. 1, pp. 1–20, 2010.

[30] S. E. Alkhatib, H. Mehboob, and F. Tarlochan, "Finite Element Analysis of Porous Titanium Alloy Hip Stem to Evaluate the Biomechanical Performance During Walking and Stair Climbing," *J. Bionic Eng.*, vol. 16, no. 6, pp. 1103–1115, Nov. 2019.